NAL PROPOSAL NO. 449

A Proposal to Measure Coulomb and Diffractive Production of K^*, $\bar{K}^*$

M. A. Abolins, B. Dodge, J. A. J. Matthews, R. A. Sidwell
Michigan State University

H. R. Barton, Jr., N. W. Reay, N. R. Stanton
The Ohio State University

K. W. Edwards
Carleton University

Correspondent:

M. A. Abolins
Michigan State University
East Lansing, Michigan 48824
Tel.: (517) 353-5180
(517) 353-1677

Abstract

We propose to study the diffractive and Coulomb production of $K^{*\circ}$, $\bar{K}^{*\circ}$'s using a K_L° beam and a variety of nuclear targets ranging from carbon to uranium. This investigation would result in

a) a precise measurement of the radiative widths of the $K^{*\circ}$, $\bar{K}^{*\circ}$

b) new information on the strong interaction diffractive mechanisms

c) a possible measurement of the radiative width of the $K^*(1420)$

We intend to use the M3 beam suitably hardened to enhance the K_L° beam component. The detector employed would be structured around our spectrometer previously used in experiment 366. The total time request is 600 hours.

I. Physics Motivation

We propose to measure the production of $K\pi$ states using the K_L° component of the M3 beam incident on a variety of targets. We summarize below the motivation behind this measurement of $K\pi$ resonances.

(A) Coulomb production

The radiative widths of the vector mesons provide important clues to understanding their substructure in terms of the quark model. At the present time the only directly measured widths are:

Table I

Process	Width (KeV)
1) $\omega^\circ \to \pi^\circ\gamma$	890 ± 70
2) $\phi^\circ \to \eta\gamma$	126 ± 45 (KeV)

Using process (1) as input, we may make predictions of several other vector meson radiative widths for which direct measurements do not exist but which have been deduced by means of the "Primakoff effect", that is production in the Coulomb field of a nucleus. We summarize these[1] in Table II.

Table II

Process	Primakoff Measurement (KeV)	Prediction (KeV)
3) $\rho^- \to \pi^-\gamma$	35 ± 10	~ 100
4) $K^{*\circ} \to K^\circ$	75 ± 35	~ 280

The two reactions (3) and (4) invariably have to be measured in the presence of strong processes leading to the same final state. Both reactions have been measured[2,3] at AGS energies where the competing strong interactions dominate the Coulomb production. The resultant difficulty of extracting the cross sections from this rather severe background reflects itself in the

substantial uncertainties quoted for the widths. The expression for the K* production via the Primakoff effect on nuclei is given by:[4]

$$\left(\frac{d\sigma}{dt'}\right)_{Coulomb} = \frac{t'}{(t'+t_{min})^2}\ 24\pi\alpha Z^2\ \frac{m_{K^*}^3}{(m_{K^*}^2-m^2)^3}\ \Gamma(K^*K\gamma)\ |F_c(t)|^2$$

where: $t' = t-t_{min}$ and $t_{min} = \left[\frac{m_{K^*}^2 - m_K^2}{2\,P_{LAB}}\right]^2$

and $F_c(t)$ is the nuclear form factor. The energy dependence is in the terms involving t_{min} and leads to a substantial increase in this cross-section (as much as an order of magnitude), in going from AGS to Fermilab energies.

The competing strong interaction is thought to be dominated by ω° exchange and can be written as

$$\left(\frac{d\sigma}{dt'}\right)_{strong} = C_{ST}\left(\frac{P_{LAB}}{P_o}\right)\quad t'e^{-Bt'}$$

This expression, referring to proton targets, is dominated by a $\approx \frac{1}{P_{LAB}}$ factor[5] giving substantial decrease by Fermilab energies. The relative cross sections from these two processes at two energies are shown in Fig. 1..

For the present experiment the Coulomb production dominates the strong and we estimate that ω° production will constitute $\lesssim$10% of the Coulomb cross section.

In this experiment we propose to measure the two reactions:

1) $K^\circ + A \rightarrow K^*(890) + A$
$\qquad\qquad\qquad\qquad\qquad\qquad\qquad\qquad\quad \rightarrow K^+\pi^-$

2) $\bar{K}^\circ + A \rightarrow \bar{K}^*(890) + A$
$\qquad\qquad\qquad\qquad\qquad\qquad\qquad\qquad\quad \rightarrow K^-\pi^+$

using the K°, $\bar{K}^\circ$ components of the K_L°'s in the neutral beam. The Coulomb

contribution to these two processes is the same. The strong interactions if mediated via ω exchange also give equal contributions. However, Pomeron exchange cannot be excluded, and could lead to differences in the two angular distributions outside the Coulomb peak. The relative phase of the Coulomb and strong amplitudes can be extracted from these measurements, a quantity to which the AGS experiments are insensitive.

An additional bonus of going to higher energies is the possibility of measuring the radiative widths of higher K* resonances such as the K*(1420). The higher momenta permit t_{min} that do not damp out high masses strongly and easily satisfy the necessary coherence conditions for production off a heavy nucleus such as Pb. Since the acceptance of our apparatus (see Fig. 2) will not be optimized for the higher mass studies we expect a substantially lower yield for this state even if the radiative widths are comparable. Our future planning in this regard awaits some results from the present experiment. Explicit rate estimates are considered in a later section.

II. Experimental Considerations

(A) Physical layout

The experimental apparatus consists of a target surrounded by a scintillator, lead, scintillator veto box followed by a vee spectrometer. The detectors before the magnet are a series of wire proportional chambers and after the magnet fourteen planes of spark chambers. This system, shown in Fig. 3, is substantially the same as that used in E-366.

Two large Cerenkov counters and a series of three hodoscopes complete the detector and these are discussed below.

(B) Cerenkov Counters

The spectrometer is constructed around two Cerenkov counters C_1, run at ~~high~~ low pressure and set to tag π's and not K's, and C_2 run at room

pressure tagging both π's and K's. Figure 4 shows realistic pressure curves for C_1 and C_2 based on our experience with such counters in E-366.

The counter C_1 is a pressure vessel 10m long and 1.5m in diameter. A horizontal septum separates it into two horizontal compartments (upstairs/downstairs). Separate mirrors focus light on RCA 31,000m photomultipliers. This counter is in its final stages of construction and is shown in Fig. 5 .

The counter C_2 is yet to be built but will be functionally identical to C_1 except filled with room pressure H_2 and will be run with a lower threshold.

The permutation of possible signals from the two counters is given in Table III. Thus, for example, a K*, $\bar{K}$* produced by a 70 GeV/c K_L^o decays into $K^+\pi^-$, π^+K^-, which are tagged N, Y and Y, N by C_1 and Y, Y by C_2. The dominant background of $p\pi^-$ at comparable momentum would typically have a proton too slow to trigger C_2. Other possible backgrounds such as $\pi^+\pi^-$ of course are vetoed by C_1. Our rate and background estimates explicitly take these considerations into account.

Table III. Cerenkov Signatures

Track Sign	Particle	C_1	C_2
	π^+	N,Y(a)	Y
+	K^+	N	Y
	p	N	N
	π^-	N,Y	Y
-	K^-	N	N,Y
	$\bar{p}$	N	N

(a) Multiple entries implies that, with track reconstruction, these tracks can be identified. The contamination from the implied $\bar{p}$, K^- ambiguity is estimated to be <20%

(C) Counter Hodoscopes

The suppression of neutron induced background is accomplished by taking advantage of the generally higher momentum distribution of the neutron vs the K_L beam. The three hodoscopes H1, H2, H3 can be used to place rough maximum momentum requirements on the outgoing particles. This scheme is explained in Appendix II. The logic imposes a minimum angle requirement which is implemented through MECL logic and is fed into the fast trigger. Various alternative logic schemes are being investigated that best accomplish these objectives.

(D) Trigger Rates and Beam Requirements

In all the considerations we assume that a beam of 10^5 K_L°/pulse accompanied by ~2 x 10^6 neutron is achievable in the M3 line. Detailed considerations of these estimates and the effects of beam hardening are relegated to APPENDIX I.

1) Coulomb production

We calculate here the rate of event production on a .20 interaction length, ~1.3 gm/cm^2 Pb rarget. Other targets are summarized in Table IV .

The Coulomb cross section for K* (890) production on lead is ~2.0 mb at a mean energy of 70 GeV/c and $\Gamma_{K^* \to K\gamma}$ = 75 KeV.

Thus we expect:

8×10^{-5} $(K^*, \bar{K}^*)/K_L^\circ$

Branching ratio $K^*, \bar{K}^* \to K^\pm \pi^*$ 2/3

Geometrical and Cerenkov acceptance averaged over beam momentum ~1/6

Yield of events/pulse $\simeq 10^5 K_L^\circ/_{Pulse} \times 8 \times 10^{-6} \times 2/3 \times 1/6$

$\simeq .09$

2) K* production through strong interactions

Previous K* production experiments have observed the following general features: (5)

a) A simple power law behavior for the cross sections, $\sigma \sim p_{inc}^{-n}$, with typical values of n: $2.0 \geq n \geq 1.0$.

b) The cross sections, σ, and to a lesser event, the power law exponent, n, depend on the channels studied. That is, at low energies $\sigma(K^+p \to K^{*+}p) \neq \sigma(K^-p \to K^{*-}p) \neq \sigma(K^\circ p \to K^{*\circ}p) \neq \sigma(\bar{K}^\circ p \to \bar{K}^{*\circ}p)$, see Figure 6a.

c) The production density matrix elements for the K* signify dominant, but not exclusive, natural parity exchange.

The K_L° beam in the M3 beam now provides a unique tool for accurately comparing the cross sections, and the production density matrix elements, for the interactions:

$$K^\circ + A \to K^{*\circ} + A$$
$$\qquad\qquad \big|\to K^+\pi^-$$

$$\bar{K}^\circ + A \to \bar{K}^{*\circ} + A$$
$$\qquad\qquad \big|\to K^-\pi^+$$

In the above, A refers to coherent production off a light nucleus, for example carbon.

We estimate the rates as follows:

a) at lower energies: $\sigma(K_L^\circ p \to K^*p) \sim 2/3\ \sigma(K^-p \to K^{*-}p)$;

b) $\sigma(K^-p \to K^{*-}p)\big|_{65\ GeV/c} \approx 10\mu b$ (see Fig. 6b);

c) for coherent production (i.e., P,f,ω° t channel exchanges), the interaction rate on C $\geq$ 1/2 H for the same absorption length target.

The rate of accepted K* events is then:

$$\text{RATE} \approx (10^5\ K_L^0/\text{pulse})\ (0.1\ \text{absorption length target})$$
$$\times \left(\frac{4.4 \times 10^{-3}\ \text{mb}\ (K_L^0 p \to K^* p)}{32\ \text{mb}\ (pp\ \text{inelastic}\ \sigma)} \times \frac{1}{2}\right)\left(\begin{array}{l}0.15\ \text{acceptance for identical}\\ K^+,\ K^-\ \text{Cerenkov cuts}\end{array}\right)$$
$$\simeq 0.1/\text{pulse}$$

This thickness target will probably result in too large a background from n associated reactions, see following section. Thus, early running on the coulomb production experiment will enable us to determine whether we can also take data at a meaningful rate on K* nuclear production.

3) Backgrounds

Even with the relatively large ratio of $n/K_L^0 \sim 20{:}1$, predicted backgrounds from both n and K_L^0 interactions appear to be within acceptable limits (except as noted above). This is achieved as a result of four factors:

a) simple event geometry with only two forward tracks;

b) the use of fast hodoscope logic to exclude events with like-charge or high momentum (e.g. $p \gtrsim 70$ GeV/c) tracks;

c) effective coverage of $\sim 4\pi$ solid angle with $\pi^0(\gamma)$ shower counters used to veto events with π^0's. We have previously built such veto walls and target boxes for experiments at Fermilab and at ANL. We estimate their efficiency at ≥90%.

d) two Cerenkov counters that allow both unique identification of $K\pi$ events and suppression of $\pi^+\pi^-$ or $p\pi^-$ backgrounds. The Cerenkov information is optimally used in conjunction with the momentum information, point b). The sources of background are itemized below.

a) $K\pi$ events from strong interactions:

As discussed above, coherent nuclear production of K*'s occurs at less than 1 event/pulse. The $K\pi$ backgrounds from other

channels will be dominated by diffractive "Q" production. In particular, the troublesome reaction is:

$$K_L^\circ p \to Qp \quad \Big| \to K_L^\circ \pi^+ \pi^-$$

where the K_L° is undetected. This cross section is 4/18 the cross section for $Q \to K^*\pi$. Using a cross section[6], $Kp \to Qp \leq 1$ mb, we estimate for 0.2 radiation length targets (corresponding typically to ~1% absorption lengths) that our trigger background from Q events is ≤5/pulse.

b) n induced backgrounds:

Estimates from exclusive reactions[7], $pp \to n\pi^+ p$, and from inclusive data on charged multiplicities[8] indicate that the cross section for a neutron to dissociate is:

$$\sigma_{n \to p\pi^-} + (m\pi^\circ\text{'s}) \simeq 1.6 \text{ mb}$$

and that

$$\sigma_{n \to p\pi^-} \simeq \frac{1}{2}\left(\sigma_{n \to p\pi^-} + (m\pi^\circ\text{'s})\right).$$

Thus, for a neutron flux of 2×10^6/pulse we expect:

$$\#\text{ of } p\pi^- \simeq (2 \times 10^6 \text{n/pulse})(\sim 1\% \text{ abs. length targets}) \left(\frac{0.8 \text{ mb}}{32 \text{ mb}} \frac{\text{cross section}}{\sigma_{pp}^{\text{abs.}}}\right)$$

$$\times (0.05 \text{ momentum hodo acceptance for } p \leq 70 \text{ GeV/c})$$

$$\times (0.5 \text{ Cerenkov cut on the + ve track})$$

$$\simeq 13/\text{pulse}$$

(E) Other

1) Resolution

The experimental geometry (see Fig.3) and choice of magnetic field in the forward spectrometer have been chosen to maintain excellent angular and momentum resolution. This is a crucial consideration in

Coulomb production experiments. The Coulomb cross section for K* production peaks at a momentum transfer $t' \sim |t_{min}| \sim 0.076/p^2_{K^\circ_L}$ GeV^2, whereas the nuclear cross section, $\frac{d\sigma}{dt} \sim t' e^{\frac{R^2 t}{3}}$, peaks at $t' \sim 3/R^2$ ($\sim 1/400$ GeV^2 on lead).

Our predicted angular resolution, $\delta\theta$, (which is dominated below 100 GeV/c by multiple scattering in the 0.2 rℓ targets) is compared to θ_{PEAK}, the angle of the maximum Coulomb and nuclear differential cross sections, in Fig. 7 . The graph shows that$(\theta_{coulomb}/\delta\theta)$ is typically ≤ 1. Thus the forward dip in the Coulomb cross section is not resolved. However,$(\theta_{nuclear}/\delta\theta)$ even on lead is typically ~4, indicating that the peak in the nuclear cross section is easily resolved. In terms of $P_\perp$, our resolution corresponds to $\delta p_\perp < 10$ ~~GeV~~ MeV/c.

2) Normalization, K°_L Decays:

We will be sensitive to the K°_L decay modes: $K^\circ_L \to \pi\mu\nu$, $K^\circ_L \to \pi e\nu$ and the convenient normalization channel $K^\circ_L \to \pi^+\pi^-$. These decays comprise ~66.5% of the K°_L decays. For 10^5 incident K°_L/pulse this results in ~13 K°_L decays/meter/pulse accepted by the spectrometer. These decays will provide our normalization as follows:

a) A decay region of 0.5m, containing the target near the upstream end, will provide a continuous source of ~6 $K_{\ell 3}$ decays/pulse. These can be analyzed to obtain the K°_L flux and spectrum shape.[9]

b) Special runs, with a $\geq$3 m evacuated decay volume, will provide a sample of CP violating decays ($K^\circ_L \to \pi^+\pi^-$). These data measure directly the spectrometer's angular resolution, and corroborate the beam flux normalization from $K_{\ell 3}$ decays.

III. Summary of Trigger Rates and Time Estimates

We list below the expected trigger rates from the various processes discussed above.

		Events/pulse
K_L	K^*, $\bar{K}^*$(Coulomb)	.09
K_L	K°, $\bar{K}^*$,(ω° exch.)	.01
Q background		5.
Neutron induced		13.
KL3 decays		6.
		24

We have previously run our proportional chamber, spark chamber spectrometer at 3 times these rates so no problem is anticipated here.

The event rate for Coulomb production .09/pulse indicates that there will be no difficulty in obtaining several hundred such events per day under normal running conditions. We would like to measure the radiative width of the K*(890) to 10% (assuming that it is ~70 kev). The limitations on this measurement will come from our ability to accurately measure the rate for this process in the presence of the strong interaction channels. The dominance of the Coulomb process in the forward direction will greatly aid us in this task.

In order to properly study the systematics of this reaction, we plan to run with a variety of nuclear targets, U, Pb, Sn, Cu, and C, and would like to get a few thousand events for each element. We therefore request 600 hours of beam time to perform this measurement.

IV. Equipment & Supplies:

A. Requests from Fermilab:

a) One BM-109 dipole opened to 10" vertical aperture (+ power supply and magnet end plates).

b) LiH (or Be) preferential absorbed of neutrons. To decrease the n flux by ~30x requires ~3 absorption lengths of LiH (~2.4 m) or Be (~1.1 m) plus the lead photon filter of ~15 r. . The LiH or Be absorbed must be remotely controlled (e.g., with the MAC system), preferentially in at least two sections of ~2 abs. length and ~1 abs. length units. Suggested locations for the absorber (ordered by preference) are:

(i) just upstream of the north wall of the meson lab target hall (i.e., upstream of 269' location);

(ii) part of the absorber (Be) in the bending magnet at 380' location, plus a remotely controlled section to replace the horizontal and/or vertical movable collimator at 388', 393'.

c) PDP11/45 Bison computer - data acquisition system (as per E366).

d) Discriminators, logic units, latches, etc., from PREP.

We estimate that our requirements here will be similar to those for E366, approximately $85,000.

e) To minimize the beam spot size, and the loss of K_L^o's through decay, we would like to set up the spectrometer as far forward as possible in the M3 beam line. To provide a K_L^o decay region, a vacuum pipe of ≃ 6" I.D. should extend ≥5 meters upstream of our target.

(B) Supplied By Experimenters

We mention below items that have yet to be constructed:

a) a room pressure H_2 Cerenkov counter

b) two hodoscopes of 4 and 48 counters

c) target veto box

d) A series of Pb-scintillator aperture baffles similar to ones used previously in E-12, np charge exchange.

e) A Pb scintillator hodoscope sandwich to veto background γ's from π^0 decays passing through the aperture of the magnet. This array would consist of two orthogonal hodoscopes separated by 1 cm of Pb. A similar system has been used by members of this collaboration in an Argonne experiment.

(C) Proposed Start of Running

A careful analysis of our construction capabilities convinces us that the necessary items for this experiment can be ready on the floor for parasitic running in March, 1976. We would propose a period two to three weeks of parasitic tuning with data taking to commence on or about April, 1976. At this time we have no other major experimental commitments.

APPENDIX I

K_L° Flux in M3 Beam

The flux of K_L° mesons expected in the M3 beam line is given by:

$$\#K_L^\circ/GeV/10^{12}p = \left(\frac{d^2\sigma}{dpd\Omega}\right)_{\substack{LAB \\ pp\to K_L^\circ + anything}} (\Delta\Omega)\, F_A\, F_D \left(\frac{(1-e^{-\ell_T/\ell_A})\, 10^{12}}{\sigma_{pp}^{inel}}\right) \qquad (1)$$

where: (1) $\Delta\Omega$ is the solid angle of the secondary beam line;

(2) ℓ_T = target length, ℓ_A = absorption length for protons on Be;

(3) σ_{pp}^{inel} is the pp inelastic cross section;

(4) F_A, F_D are the K_L° attenuation factors from secondary interactions and from K_L° decays respectively.

To estimate $\left(\frac{d^2\sigma}{dpd\Omega}\right)_{pp\to K_L^\circ}$ we assume

$$(pp \to K_L^\circ) = (pp \to K_S^\circ) \approx 1/2(pp \to K^+ + pp \to K^-)$$

Thus, with:

$$\left(\frac{d^2\sigma}{dpd\Omega}\right)_{LAB} = \frac{p^2}{\pi}\left(\frac{d^2\sigma}{dp_{11}dp_\perp}\right)_{LAB} = \frac{p^2}{\pi p_{MAX}}\left(\frac{d^2\sigma}{dxdp_\perp^2}\right)_{LAB}$$

$$= \frac{p^2}{\pi p_{MAX}}\left(\frac{d^2\sigma}{dxdp_\perp^2}\right)_{CM}$$

and $$E\frac{d^3\sigma}{d\vec{p}^3} = f(x,p_\perp^2) = \frac{E^*}{\pi p_{MAX}^*}\left(\frac{d^2\sigma}{dxdp_\perp^2}\right)_{CM}$$

we obtain: $$\left(\frac{d^2\sigma}{dpd\Omega}\right)_{LAB} \approx \frac{p^2}{E}\, f(x,p_\perp{}^2) \approx pf(x,p_\perp{}^2) \qquad (2)$$

A reasonable parameterization for the K_L° Lorentz invariant differential cross section is given by:[8,10]

$$f(x,p_\perp^2)_{pp\to K_L^\circ} \simeq 4.5\, e^{-7.7|x| - 4.5p_\perp^2}\ \text{mb/GeV}^2 \quad \text{for } |x| \geq 0.15.$$ For

$|x| < 0.15$ this function slightly overestimates the K_L° yield.

Analogous predictions can be made for the neutron flux. Using the inclusive cross sections of ref. 11, and taking a production angle of the M3 beam of 0.5 mr , we obtain reasonable agreement with the measured neutron flux at 300 GeV/c. This is shown in Fig. 8 , where a comparison is made of the shape of the predicted and measured[12] spectra. The n flux has been normalized to the observed[13] flux at 300 GeV/c. The flux normalization is not as good, the predicted flux beingapproximately a factor of two high. The final n, K_L° normalizations have been set by the observed n flux and the measured K_L°, n composition of the beam[14] at 300 GeV/c.

Predicted fluxes at 400 GeV/c (per 10^{12} protons), and with a M3 beam solid angle $\Delta\Omega = 9.4 \times 10^{-9}$ sr (3/4" square collimator at 647 feet), are then:

	no absorber	n attenuated by 30 x
n	1.8×10^7	0.60×10^6
K_L°	2.0×10^5	0.31×10^5
K_L°/n ratio	1.1%	5.2%

We assume the secondary absorber in the beam is a low A material, preferably LiH or Be with $\sigma_n{}^{inel}/\sigma_{K_L^\circ}{}^{inel} \geq 1.8$.[15] These rates suggest that an adequate K_L° flux, $\sim 10^5$/pulse, and K_L°/n ratio $\sim$ 5%, is attainable for $\sim 3 \times 10^{12}$ protons on the meson target. The predicted yield curves for this beam are shown in Figure 8 .

APPENDIX II

Fast Hodoscope Logic

The distances of the counter hodoscopes relative to the magnet have been chosen to be multiples of each other to facilitate fast momentum reconstruction.

Interval	Distance	Ratio/90
H1 to Mag. center	270	3ℓ
Mag. Center to H2	90	1ℓ
H2 to H3	540	6ℓ

Also the counter sizes have simple relationships

Counter	Width (δ)	# Counters
H1	1/2"	4
H2	1"	24
H3	2"	24

Since three points through a magnetic field are sufficient to define a momentum, the selection of appropriate counter combinations can yield sign determination, and a momentum cut.

Using the above dimensions it can readily be shown that the bend angle through the magnet is given by

$$1) \quad \theta = \frac{\delta}{9\ell} \{ 8(n_3-n_2) + 2(n_1-n_2) + n_1 + 22.5 \}$$

And the momentum is then

$$2) \quad P = \frac{1620\ P_1^M}{[8(n_3-n_2) + 2(n_1-n_2) + n_1 + 22.5]}$$

If $P_{\perp}^{M} \approx .7$ GeV/c,

then the maximum detectable momentum ≈ 250 GeV/c

and a 100 GeV/c threshold implies typically a displacement of 2 counters. Detailed Monte Carlo studies show that a rather clear momentum cut is achieved in this manner.

Various means exist to implement the logic requirements of (1). Preliminary analysis indicates that such a scheme can be readily effected by means of MECL logic in times less than 100 nsec.

Since the proper operation of such a device is crucial to the experiment, we are also considering means whereby this instrument may be tested by computer between beam pulses.

Table IV. Targets

Material			0.2 Radiation Length[a]	
	Z	A	(cm)	Absorption length for neutrons (%)
C	6	12	13.4	26.8
Al	13	27	1.80	4.8
Cu	29	64	0.29	2.0
Sn	50	119	0.24	1.0
Pb	82	207	0.11	0.6
U	92	238	0.06	0.5

(a) Coulomb production rates are approximately constant for the same radiation length target.

REFERENCES

1. See for example: A. Bramon, M. Greco, Phys. Lett. 48B, 137 (1974); L. Brown, H. Munczek. P. Singer, Phys. Rev. Lett. 21, 707 (1968); A. Dar, V. Weisekopf, Phys. Lett. 26B, 670 (1968).
2. B. Gobbi et al., Phys. Rev. Lett. 33, 1450 (1974).
3. W. Carithers et al., Phys. Rev. Lett. 35, 349 (1975).
4. A. Halprin, C. Andersen, H. Primakoff, Phys. Rev. 152, 1295 (1966); S. Berman, S. Drell, 133, B791 (1964); L. Stodolsky, Phys. Rev. 144, 1145 (1966); G. Morpurgo, Il Nuovo Cimento 31, 569 (1964); G. Faldt, Nucl. Phys. B43, 591 (1972).
5. Y. Antipov et al., "Production of $K^{*-}(890)$ and $K^{*-}(1420)$ in the Reaction $K^-p \to (K\pi)^-p$ at 25 and 40 GeV/c," CERN preprint (1973); J. Carney et al., CERN preprint CERN/D.PhII/Phys. 72-47 (1972); R. Barloutaud et al., Phys. Lett. 38B, 257 (1972).
6. G. Brandenburg et al., Nucl. Phys. B45, 397 (1972); H. Bingham et al., Nucl. Phys. B48, 589 (1972); E. Bracci et al., "Compilation of cross sections II - K^- and K^+ induced reactions," CERN/HERA 72-2 (1972).
7. E. Bracci et al., "Compilation of cross sections III - p and $\bar{p}$ reactions," CERN/HERA 73-1 (1973); S. Mukhin, V. A. Tsarev, "Recent Results on Nucleon Diffractive Dissociation," Fermilab-Conf-74/97-THY/EXP (1974).
8. J. Whitmore, Phys. Reports 10C, 273 (1974).
9. See for example: G. Brandenburg et al., Phys. Rev. D7, 708 (1973); G. Brandenburg et al., Phys. Rev. D8, 1978 (1973).
10. P. Capiluppi et al., Nucl. Phys. B70, 1 (1974); M. Albrow et al., Nucl. Phys. B56, 333 (1973); M. Albrow et al., Nucl. Phys. B73, 40 (1974).

11. J. Engler et al., "Measurement of Inclusive Neutron Spectra at the ISR," CERN preprint (1974); with noted normalization problems: B. Robinson et al., Phys. Rev. Lett. 34, 1475 (1975); J. Engler et al., Nucl. Phys. B64, 173 (1973).

12. Fermilab Experiment 305: B. Gobbi et al.

13. Fermilab Experiments 12, 366: M. Abolins et al.

14. P. Murthy et al., Nucl. Phys. B92, 269 (1975).

15. W. Lakin et al., Phys. Lett. 31B, 677 (1970).

FIGURE CAPTIONS

1. Coulomb and ω exchange contributions to K*(890) production on Pb at 8 and 70 GeV/c.

2. K_π acceptance averaged over the K_L° beam spectrum (Fig. 8). The acceptance for K_π events with momenta $\leq$ 70 GeV/c/track, as determined by the hodoscope logic (see APPENDIX II), is shown dashed. Cerenkov cuts typically reduce these acceptances by ~1/3 to 1/2.

3. Schematic of our proposed forward spectrometer. The γ veto counters are only shown in the plan view.

4. (a) Cerenkov threshold curves with realistic efficiencies included. Cerenkovs C_1 and C_2 would typically run with indices of refraction approximately that of He and H_2 respectively.
   (b) Actual pressure curve for Cerenkov counter (similar to C_1) used in E-366

5. Engineering drawing the main body of Cerenkov C_1.

6. (a) Low energy $Kp \rightarrow K^*p$ hadronic cross sections.
   (b) Energy dependence of $Kp \rightarrow K^*p$ hadronic cross sections.

7. Comparison of the angular resolution of the spectrometer ($\delta\theta$) to physically relevant angles:

   $\theta_{Peak}^{Nuclear}$ defining the maximum in the differential cross section for K* hadronic production, and

   $\theta_{Peak}^{Coulomb}$ defining the maximum in the K* Coulomb production differential cross section.

8. Predicted n and K_L° beam spectra at 300 and 400 GeV/c (see discussion in APPENDIX I) assuming 3 x 10^{12}p on the meson lab target, plus ~3.4 absorption lengths of LiH (Be) in the beam.

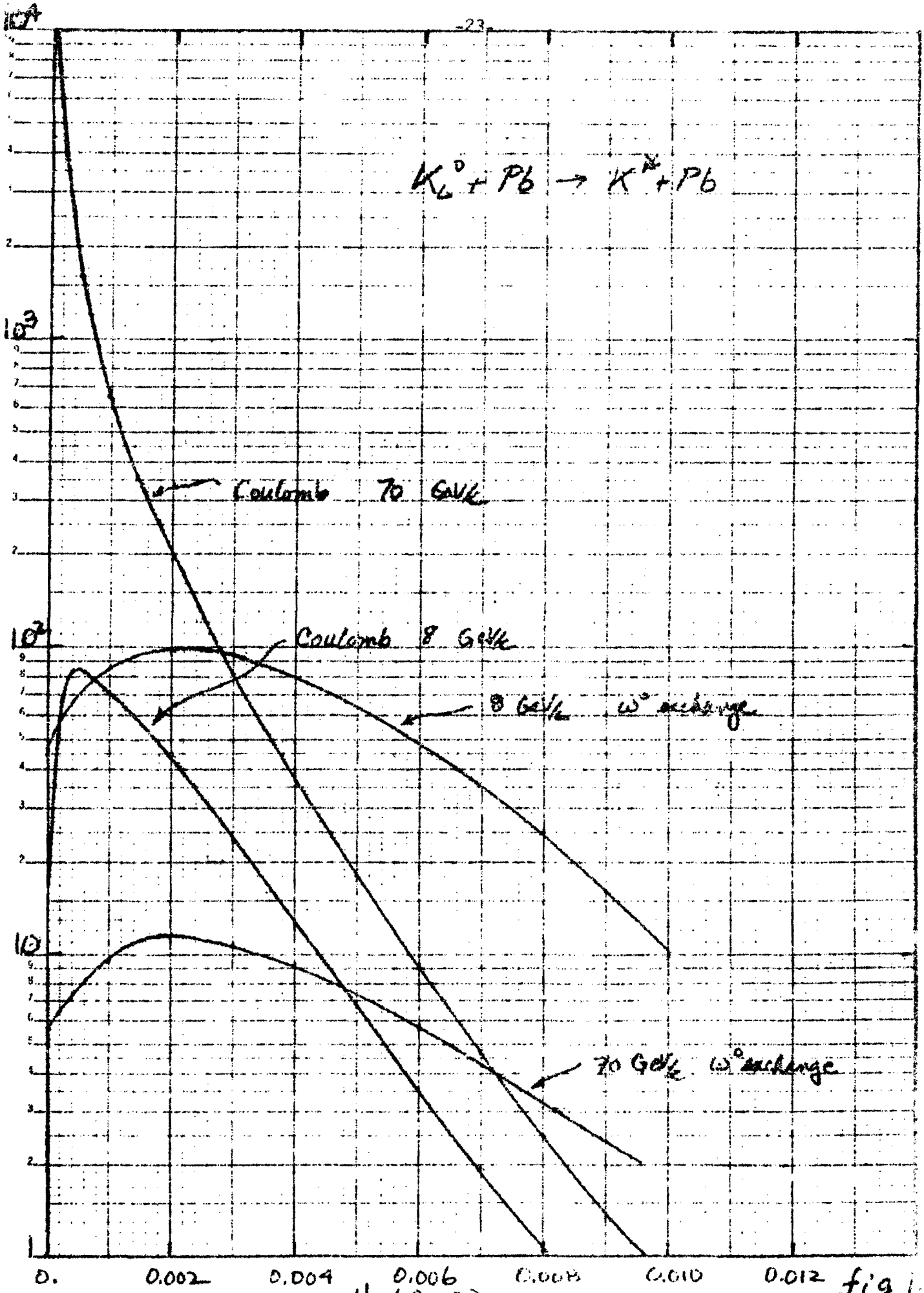
$K_L^0 + Pb \rightarrow K^+ + Pb$
Coulomb 70 GeV/c
Coulomb 8 GeV/c
8 GeV/c ω° exchange
70 GeV/c ω° exchange
$\frac{d\sigma}{dt'}$ (mb/GeV²)
t' (GeV²)
0.
0.002
0.004
0.006
0.008
0.010
0.012

fig 1

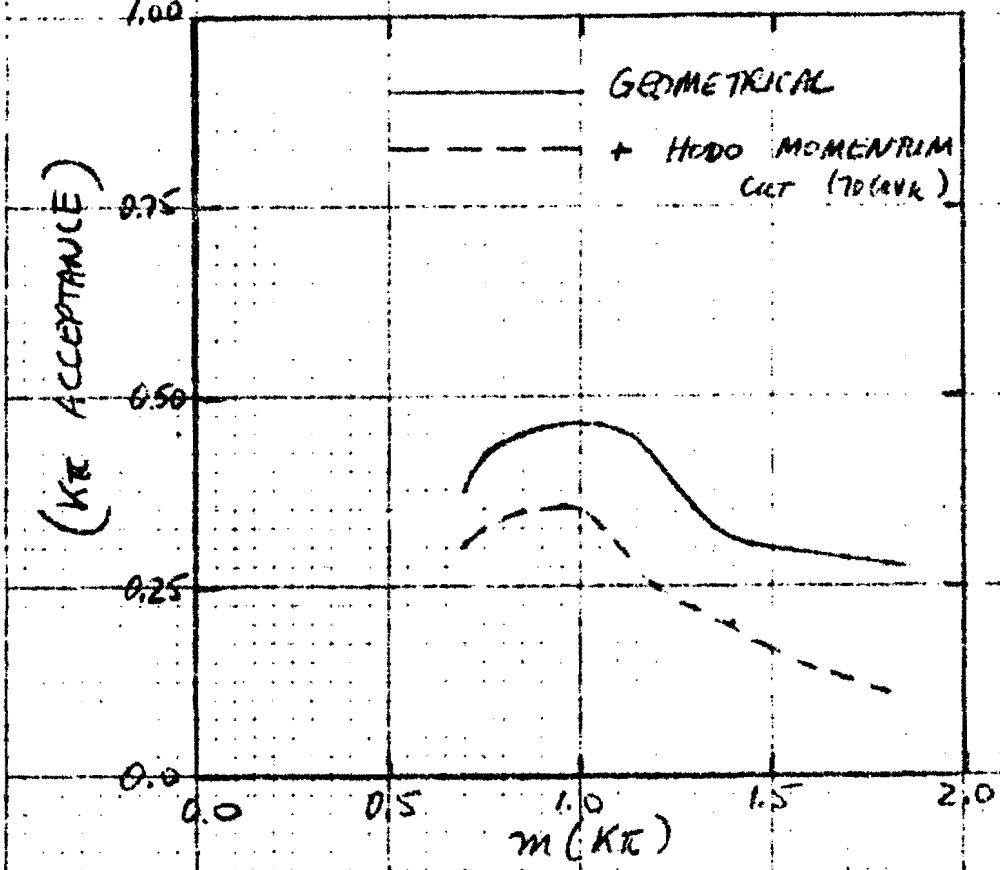
1.00
0.75
0.50
0.25
0.0
(Kπ ACCEPTANCE)
GEOMETRICAL
+ HODO MOMENTUM CUT (7 GeV/c)
0.0
0.5
1.0
1.5
2.0
m(Kπ)

fig 2.

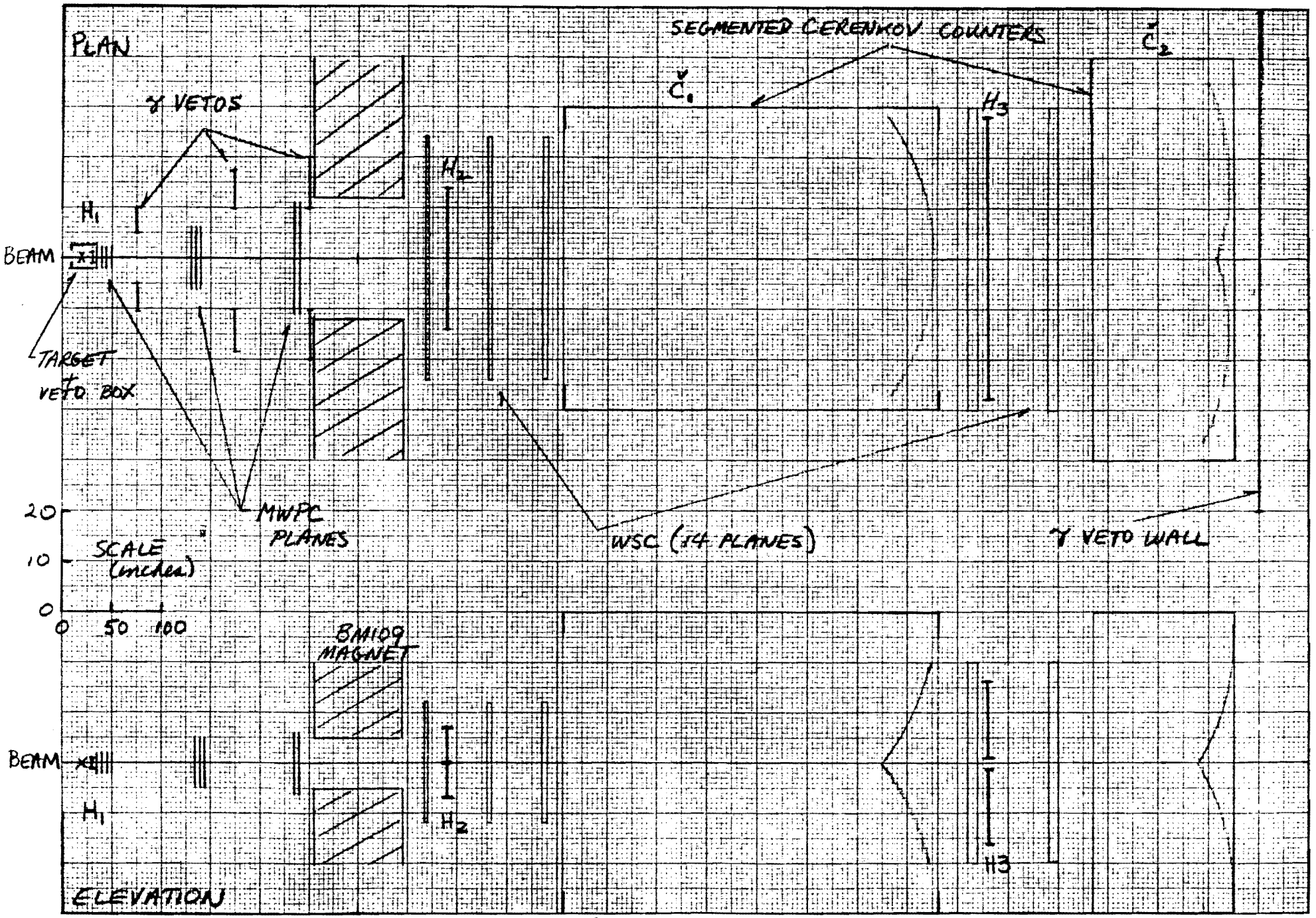

fig 3

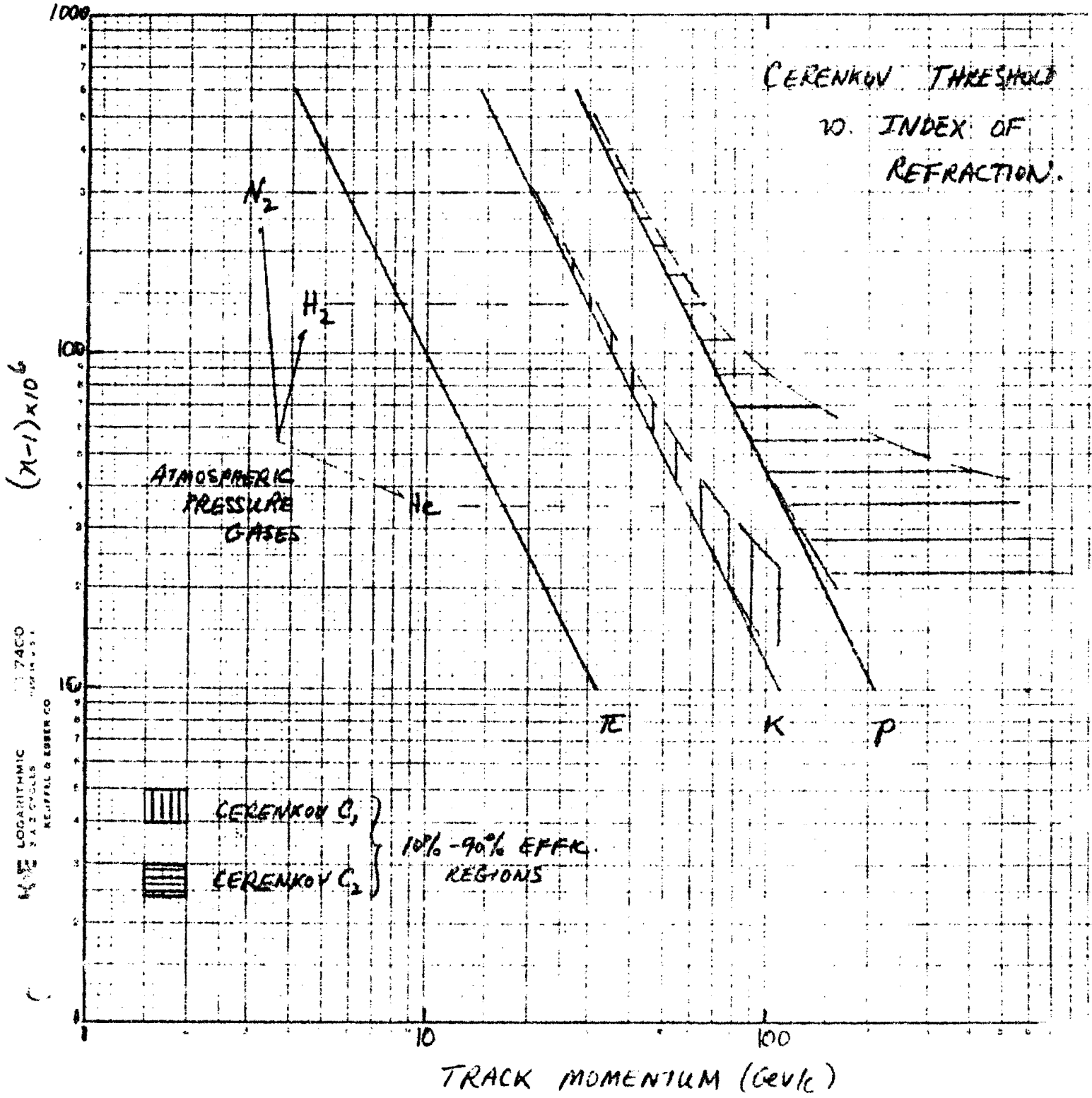
CERENKOV THRESHOLD
VS. INDEX OF
REFRACTION.
N_2
H_2
He
ATMOSPHERIC
PRESSURE
GASES
π
K
P
CERENKOV C_1
CERENKOV C_2
10% - 90% EFFIC.
REGIONS
$(n-1)\times10^6$
1000
100
10
1
10
100
TRACK MOMENTUM (GeV/c)
LOGARITHMIC
7460

fig 4a.

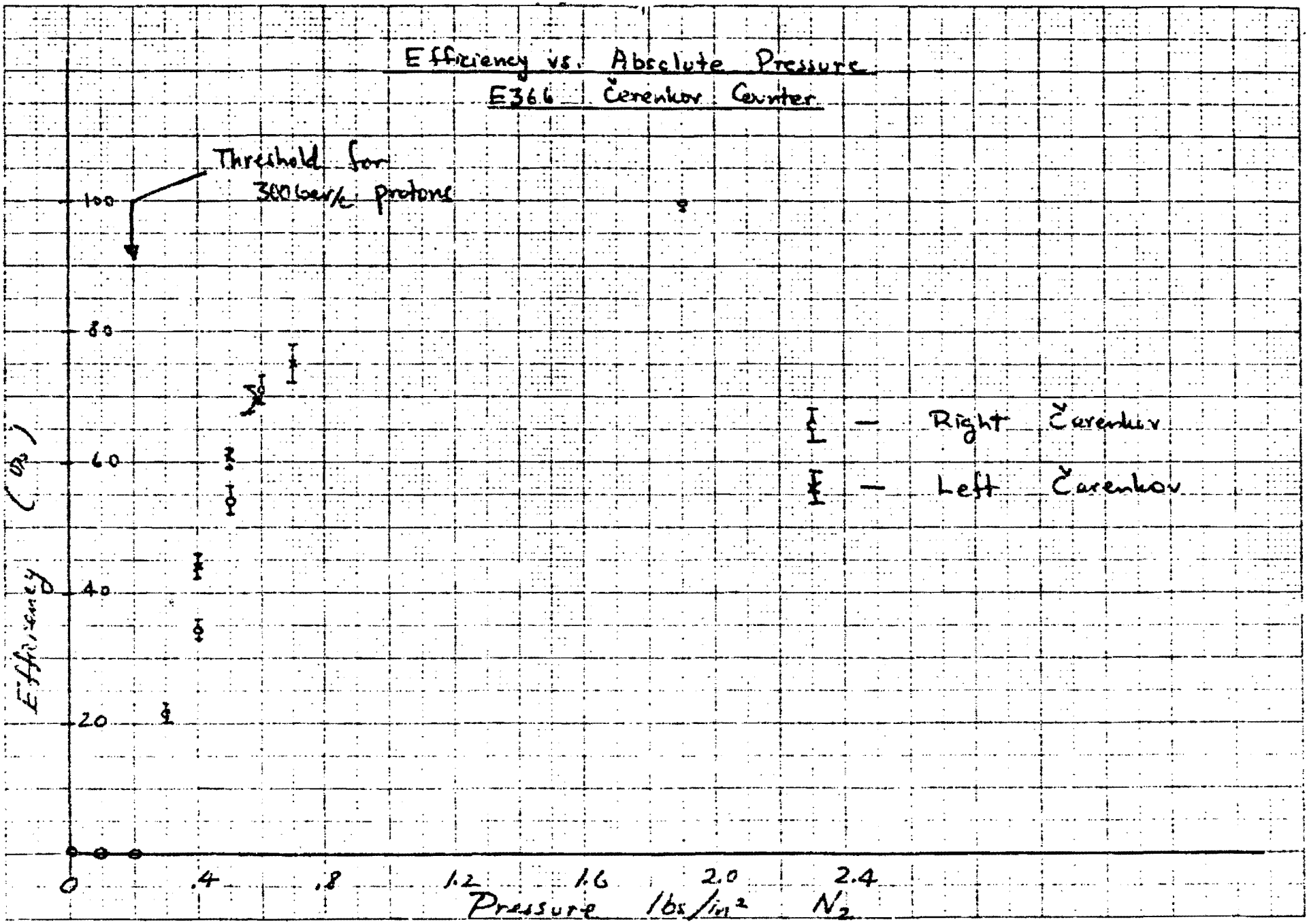
Efficiency vs. Absolute Pressure
E366 Čerenkov Counter
Threshold for
300 Mev/c protons
100
80
60
40
20
0
Efficiency (%)
.4
.8
1.2
1.6
2.0
2.4
Pressure lbs/in² N₂
Right Čerenkov
Left Čerenkov

Fig 4b.

drawing 1

material: 10/20 carbon steel
all seams welded
gas-tight

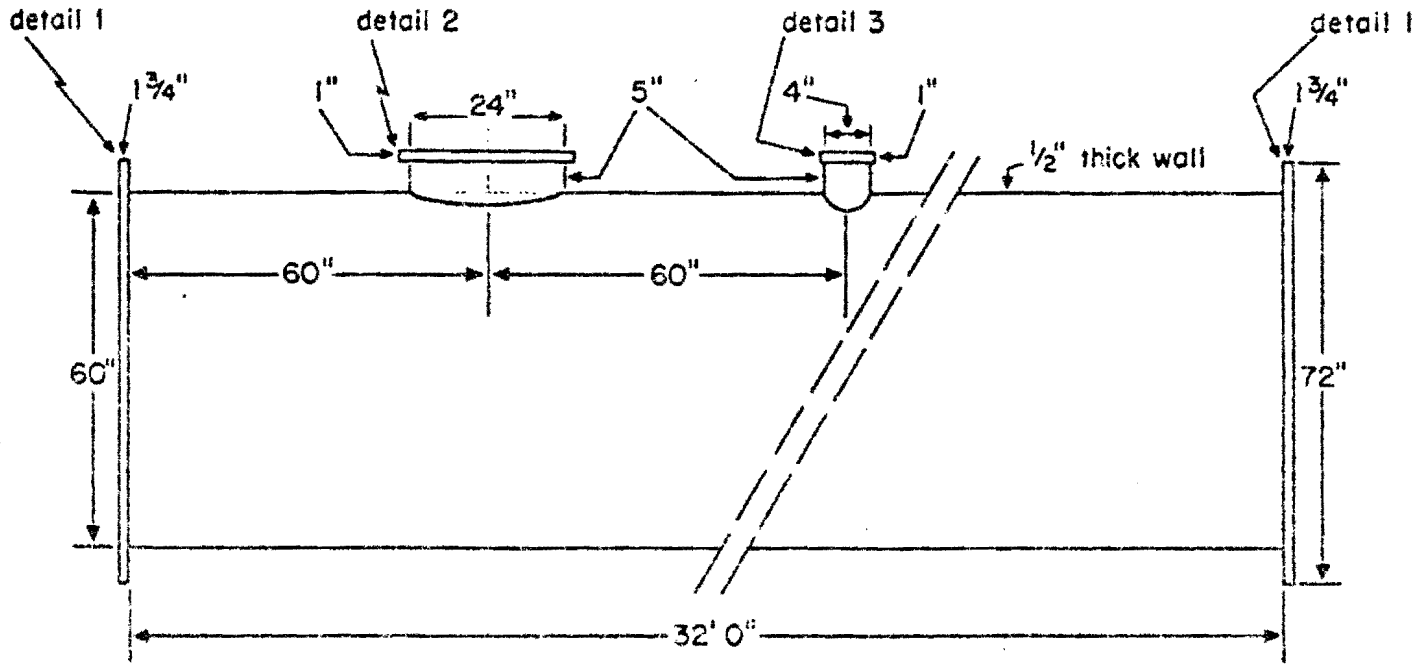

fig 5.

COMPARISON OF $K^*(890)$ PRODUCTION

$$\sigma_i = A_i \, P_{LAB}^{-n}$$

$$n = 2.00 \pm 0.10$$

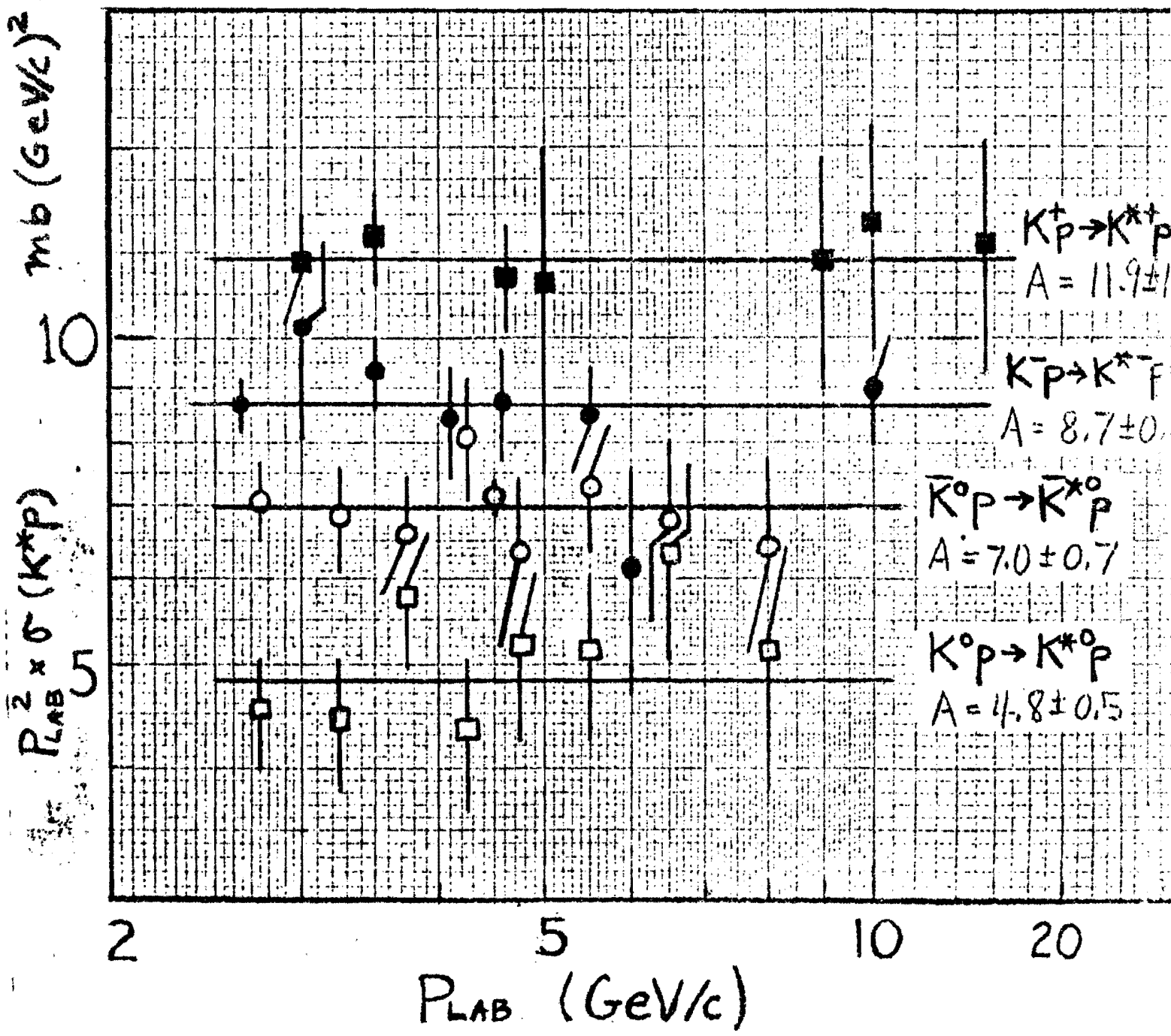

fig 6a.

Energy dependence of K^{*-}_{890} and K^{*-}_{1420} production

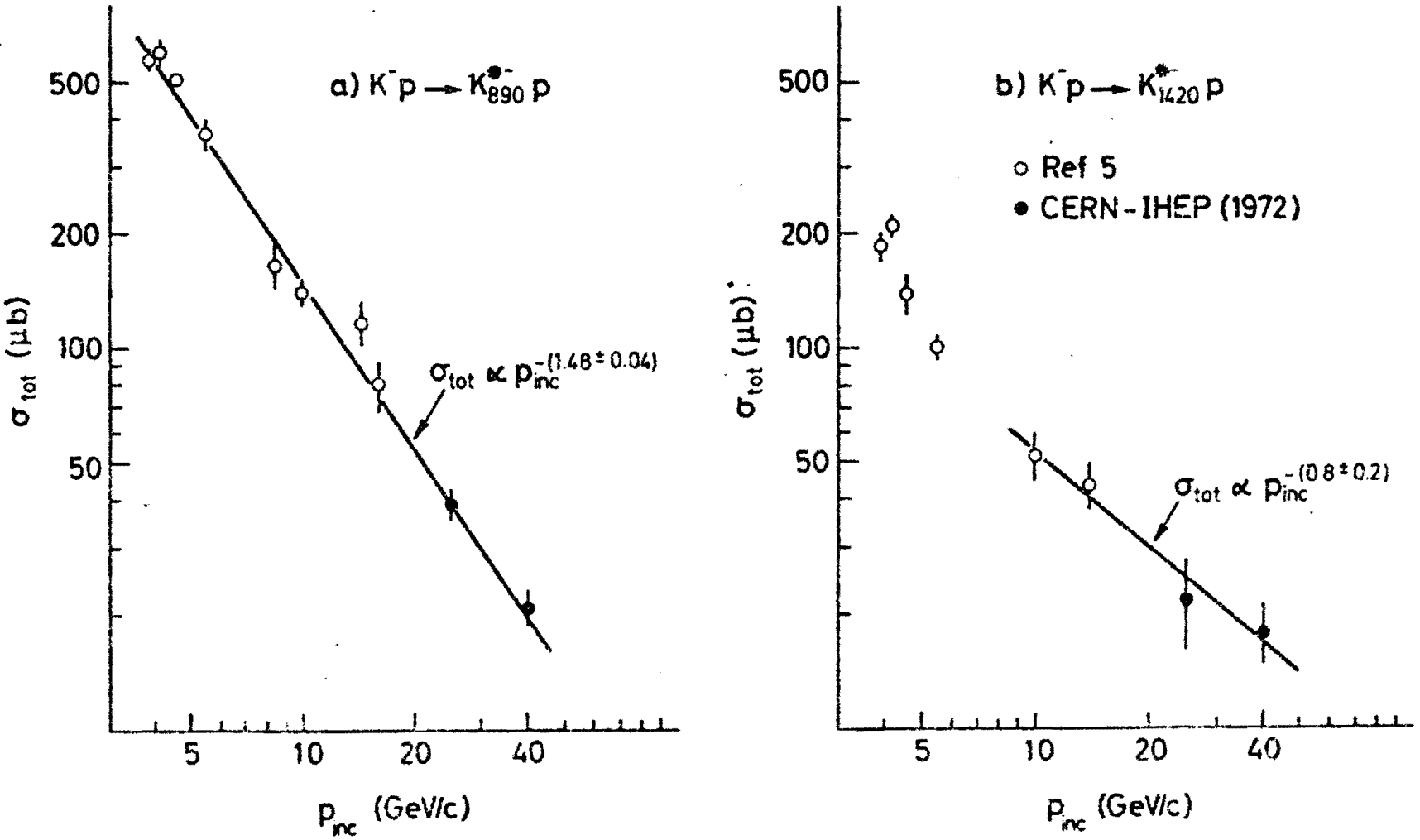

fig 6b.

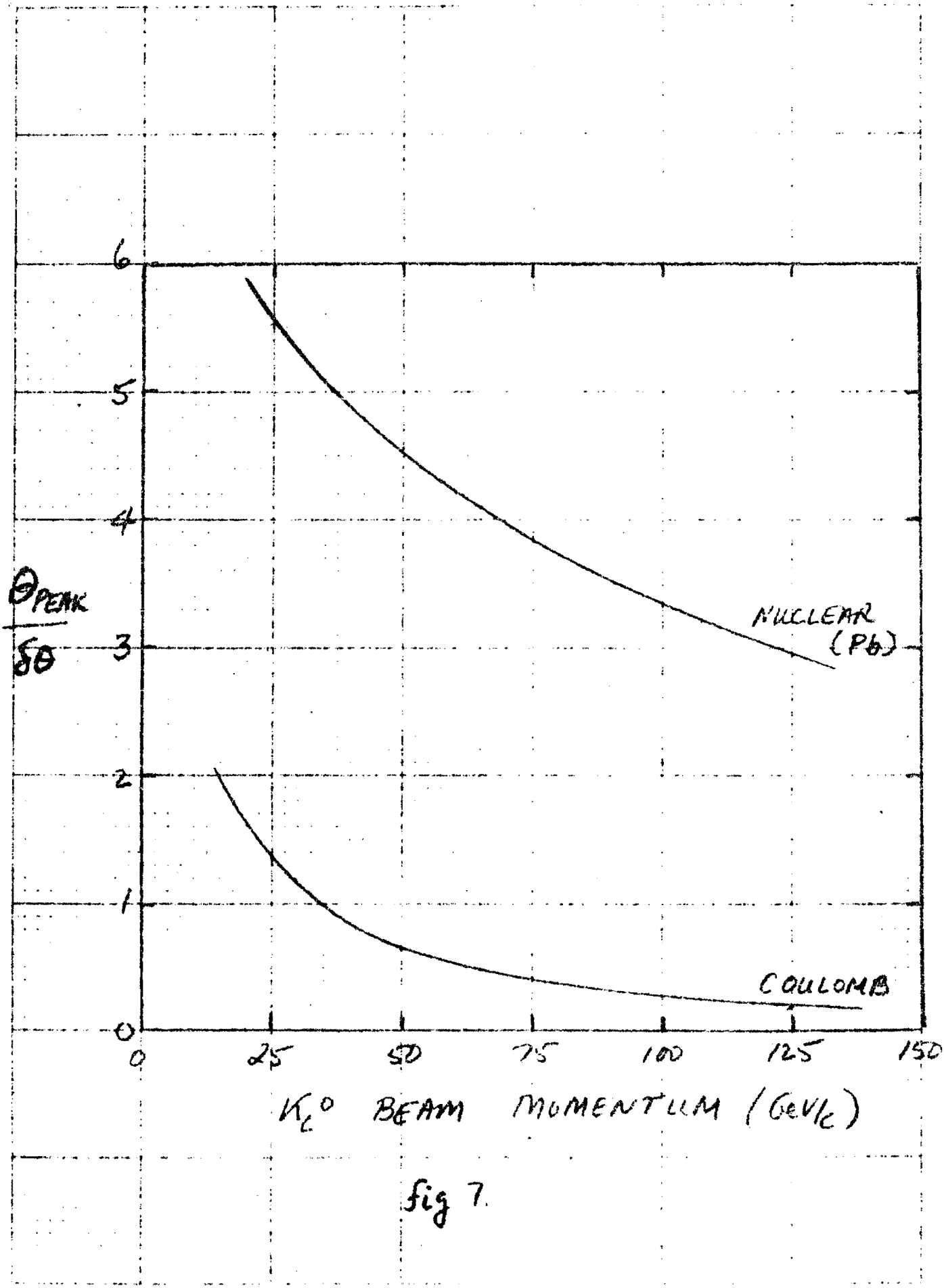
6
5
4
3
2
1
0
θ_{PEAK} / $\delta\theta$
NUCLEAR (Pb)
COULOMB
0
25
50
75
100
125
150
K_L^0 BEAM MOMENTUM (GeV/c)

fig 7.

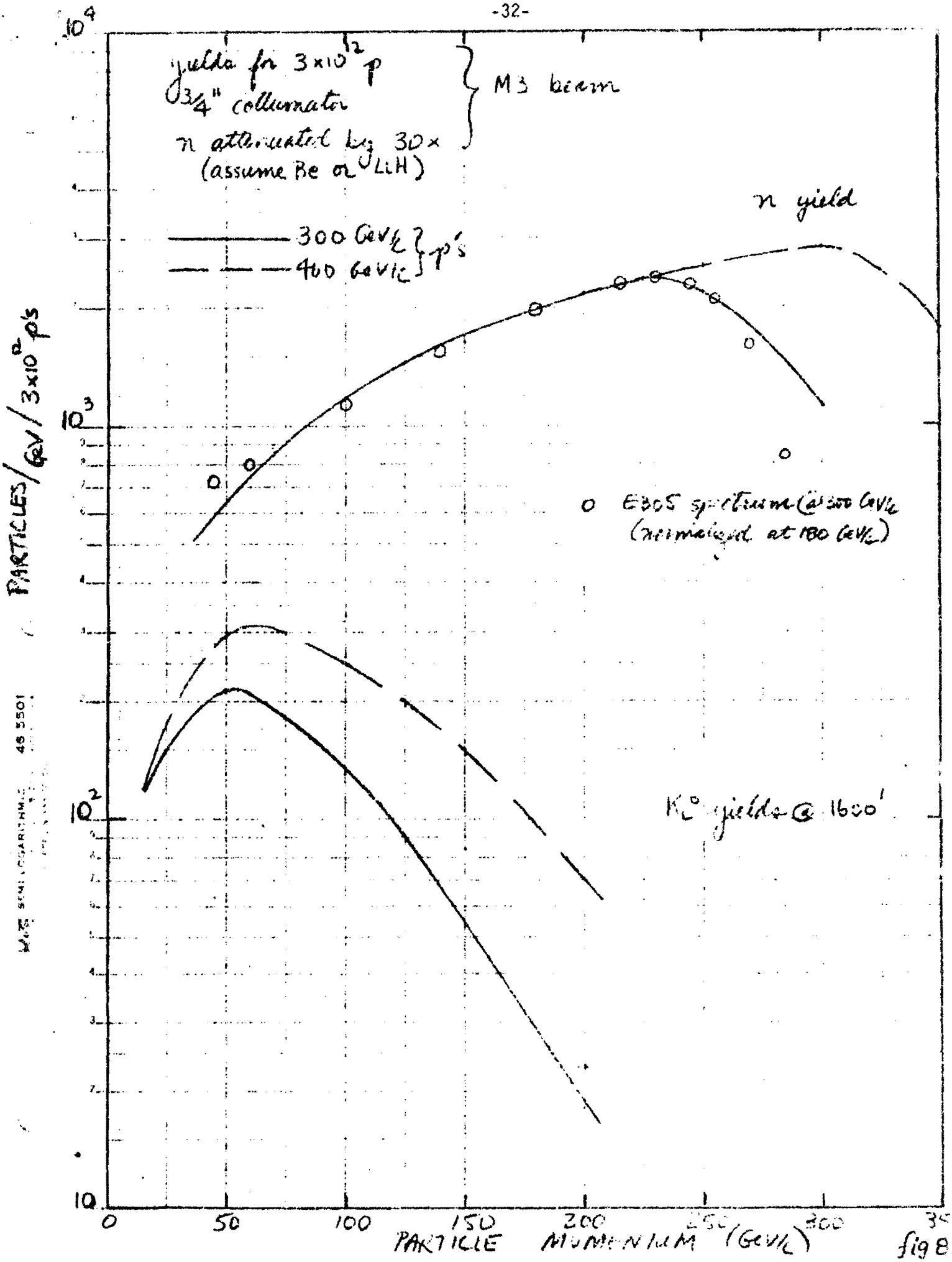
yields for 3×10^{12} p
3/4" collimator
n attenuated by 30×
(assume Be or LiH)
M3 beam
300 GeV/c
400 GeV/c
p's
n yield
o E605 spectrum @ 300 GeV/c
(normalized at 180 GeV/c)
K_L^0 yields @ 1600'
PARTICLES/GeV/3×10^{12} p's
PARTICLE MOMENTUM (GeV/c)
10^4
10^3
10^2
10
0
50
100
150
200
250
300
fig 8.